scientific reports

Check for updates

OPEN

Exploiting the mechanical properties and optimising wear characteristics of Mg–Al–Zn hybrid composites reinforced with Si_3N_4 and MoS_2

G. Anbuchezhiyan[1], M. Vignesh[2]✉, Elango Natarajan[3], Nabisab Mujawar Mubarak[4]✉, M. Sathishkumar[2] & P. Bharathi[5]

The advancement of lightweight structural materials with enhanced wear resistance continues to be a significant problem for magnesium-based alloys exploited in engineering applications. This research investigates the constraints of mechanical integrity and subpar tribological performance in Mg–Al–Zn alloys by integrating Si_3N_4 and MoS_2 hybrid reinforcements through a powder metallurgy approach. The effect of reinforcement content on density, hardness, and compressive strength was assessed, and wear behaviour was optimised through a Taguchi L9 orthogonal array to determine the main variables influencing the tribological responses. Three different trials (1–3) were used to analyse the mechanical properties with varied processing parameters, and its microstructure and mechanical properties were analysed as per ASTM standards. The microstructure observation revealed that trial 1 (Mg–Al–Zn alloy + 2 wt% Si_3N_4 + 2 wt% MoS_2) and trial 2 (Mg–Al–Zn alloy + 4 wt% Si_3N_4 + 2 wt% MoS_2) showed Si_3N_4 and MoS_2 particles agglomerating in the Mg alloy due to lower surface energy, while trial 3 (6 wt% of Si_3N_4, 2 wt% of MoS_2) exhibited a refined grain structure and acted as nucleation sites for grain refinement during sintering. SEM morphology inferred that the ceramic particles are uniformly distributed in trial 3 comprising of MoS_2, 510 °C of sintering temperature, 2.5 h soaking time, 550 MPa compaction pressure, improving mechanical properties such as hardness (43.47 ± 0.1%), compressive strength (51.16 ± 0.2%), and corrosion resistance (30.86 ± 0.01%) compared to trials 2, 3, and the Mg–Al–Zn alloy. XRDA confirms that due to higher sintering temperatures, Mg alloy interacts with ceramic particles to form the Mg_2Si, Mg_3N_2 interface. The intermixture's enhanced particle diffusion and bonding resulted in improved corrosion resistance. ANOVA analysis confirmed that Trial 3 confirmed that applied load significantly influences wear rate and CoF, with a contribution exceeding 90% and $p < 0.05$ in CoF analysis, followed by sliding speed and distance.

Keywords Powder Metallurgy, Si_3N_4/MoS_2 reinforcement , Sustainable Processing, Hardness, Corrosion, ANOVA

Mg–Al–Zn alloys are primarily used for automotive and marine applications due to its low density, high strength, formability, and castability properties at room temperature; however, at high temperatures, recrystallization occurs, coarsens the grain structure, lower strength and hardness[1]. Hybrid ceramic particles in Mg–Al–Zn alloys overcome these obstacles[2]. Several studies used various hard ceramides with dissimilar processing methods, but few used powdered sintering due to magnesium's low melting point and reactivity, which forms undesirable

[1]Department of Mechanical Engineering, Vel Tech Rangarajan Dr. Sagunthala R&D Institute of Science and Technology, Chennai, TamilNadu, India. [2]Department of Mechanical Engineering, Amrita School of Engineering, Amrita Vishwa Vidyapeetham, Chennai, India. [3]Faculty of Engineering, Technology and Built Environment, UCSI University, Kuala Lumpur, Malaysia. [4]Department of Chemical Engineering, College of Engineering, Imam Mohammad Ibn Saud Islamic University (IMSIU), Riyadh 11432, Saudi Arabia. [5]Department of Mechanical Engineering, Rajalakshmi Institute of Technology, Chennai, TamilNadu, India. ✉email: m_vignesh@ch.amrita.edu; MNSMujawar@imamu.edu.sa

oxide layers on the powders' surfaces, affecting composite properties. SiC reinforced AZ91D magnesium composites were fabricated through the application of binder jetting additive manufacturing methodologies. The enhancement of the physical and mechanical properties of the Mg-matrix composites was noted as a result of the influence of grain refinement[3]. This research clarifies the different reinforcements present in magnesium composites that underwent sintering, along with an examination of their impacts on improving wear resistance, corrosion resistance, and mechanical strength. It was observed that applying a pressure of 450 MPa, in connection with sintering temperatures between 550 and 600 °C and durations of 2 h, is recommended for achieving improved mechanical performance[4]. The Cr–Co–Ni particle-reinforced AZ31 magnesium matrix composite (CrCoNi/AZ31) was made using powder metallurgy. Hot compression tests were used to study how the microstructure of these composites changed when they were compressed and deformed at high temperatures. The $Al1_3Cr_2$ phase was seen to assist with dislocation gathering, which improved the composite material's microstructural consistency[5]. The composites of nano-SiC/Mg-8Al-1Sn (nano-SiC/AT81), reinforced with nano-SiC particles, were effectively synthesised using the powder metallurgy technique. It was noted that the compressive properties exhibited an initial enhancement with increasing nano-SiC content, followed by a decline once the nano-SiC concentration surpassed 0.50 vol%[6]. Powder metallurgy with a multitude of sintering methods was used to create B_4C/Mg composites, and it was noted that the spark plasma sintering process improves mechanical characteristics[7]. The impact of sintering temperature on the mechanical behaviour of Zn_2Mg_6SiC composites was examined and found that densification was significant at 450 °C[8,9]. Micro- and nano-alumina-reinforced Mg composites were sintered using powder metallurgy, and mechanical characteristics were significantly affected at 450 °C[10,11]. The literature on sintering magnesium inferred that the temperature influences atom diffusion, grain boundary displacement, and material densification. Excessive or uneven heating and cooling of Mg can cause thermal stress, deformation, and cracking[12]. Further, several researchers have been focused on applying the Taguchi method in combination with Analysis of Variance (ANOVA) to investigate influential process parameters, including sliding speed, applied load, and sliding distance, with the intent to define the optimal parameters that strengthen wear properties[5,13]. Therefore, the literal investigations suggest that determining the ideal temperature and reinforcing particles is crucial for minimizing thermal stress and ensuring the integrity and stability of composite structures, which is a fundamental concern. Consequently, the performance of synthesised Mg–Al–Zn alloy composites must be investigated and assessed to confirm their efficacy. It is vital to further investigate the wear properties of such alloys to optimize their performance in functional applications, where surface interactions are of fundamental importance for tribological applications[14,15].

Even though Si_3N_4 and MoS_2 have been discussed as reinforcements in numerous metal-matrix systems, there is no literature that examines their behaviour together in an Mg–Al–Zn matrix produced using an optimized powder metallurgy process. The existing literature primarily addresses individual hard particles or a given solid lubricant without describing its combined effect on densification, microstructural stability, interfacial bonding or mechanical strength and tribological performance. The current work provides an obvious novelty as it shows that a synergistic effect occurs between Si_3N_4, improving the load-bearing capacity and hardening of the matrix, and MoS_2, which helps to create a stable, lubricious tribofilm that significantly lowers friction and wear. This dual reinforcement strategy, along with the optimized compaction-sintering conditions used in our study, provides new insights into hybrid-reinforcement interactions and establishes a distinct process-structure-property relationship that has not been reported in earlier literature.

The innovation of the current work is to illustrate the simultaneous addition of Si_3N_4 (2 wt%, 4 wt%, and 6 wt%) and retaining 2 wt% MoS_2 to powder consolidation using a vacuum furnace, and their optimum process parameters and wear characteristics need to be evaluated. This is due to the identical thermal expansion coefficients, which preclude large dimensional changes at different temperatures, and blending them leads to a specific microstructural reaction, which is impossible to attain when single reinforcements are used. Even so, the challenge in combining these composites involves ensuring uniform dispersion, minimizing reactivity, and ensuring optimum densification, which are perceived as the critical features of current investigations. For this notable intention, these composites must be synthesized, and their microstructure, mechanical and wear properties need to be explored for high-strength and corrosion-resistant applications.

Materials and methods

Material selection

This experiment includes the utilization of alloying elements that involve Mg–Al–Zn owing to their low melting points, process compatibility, which facilitates lower sintering temperatures. The presence of magnesium (Mg) and zinc (Zn) in the aluminium matrix facilitates solid solution strengthening, improving hardness and tensile strength. These properties are crucial for applications that demand reduced weight and superior mechanical durability[14]. Moreover, these alloys inherently develop a protective oxide layer (Al_2O_3), which acts as a barrier against further oxidation and corrosion, making them an important choice for matrix materials. The chemical constituents of the various alloying elements are detailed in Table 1.

Si_3N_4 and MoS_2 were used as ceramic reinforcement with particle sizes of ≤ 5 µm to increase the strength-to-weight ratio. Si_3N_4 is a resilient ceramic substance characterized by a high melting point, limited thermal expansion, and exceptional mechanical strength. MoS_2 possesses outstanding solid lubricating characteristics,

Elements	Al	Zn	Mn	Si	Cu	Fe	Mg
% of Composition	0.1	0.015	0.005	0.003	0.0015	0.001	Balance

Table 1. Chemical constituents of Mg–Al–Zn alloy elements.

minimizing friction within the material and facilitating the machining and forming of magnesium composites. The combination of magnesium with these ceramic reinforcements has the potential to produce materials that are light, robust, resistant to wear and corrosion, and well-suited for the rigorous environments found in aerospace, automobiles, and biomedicine.

Powder metallurgy processing of Si_3N_4/MoS_2/Mg–Al–Zn composites

A cylindrical bowl was filled with the necessary quantity of preheated Mg and its alloying substances, ceramic and solid lubricant powders of varying weight proportions like different samples such as A (Mg–Al–Zn alloy + 2 wt% Si_3N_4 + 2 wt% MoS_2), B (Mg–Al–Zn alloy + 4 wt% Si_3N_4 + 2 wt% MoS_2), and C (Mg–Al–Zn alloy + 6 wt% Si_3N_4 + 2 wt% MoS_2), which were weighed according to the rule of mixtures. To ensure homogeneous dispersion, these mixtures are swirled at a low-speed stirrer at 300 rpm for 20 min. The mixture was subsequently positioned in a warm (130 ± 5 °C) cylindrical die measuring 30 mm × 20 mm, and a pressure of 350 MPa was applied for green compaction[16,17]. The pyrophoric nature of Mg and its interaction with the environment might result in the formation of MgO, which can negatively impact the characteristics of the sintered material. Hence, sintering was conducted within a vacuum furnace under meticulously regulated conditions, encompassing variables such as temperature (ranging from 500 °C to 800 °C) and heating rates (spanning from 5 to 20 °C/min). In the realm of pressure factors, vacuum sintering emerges as a process that operates under conditions of low pressure and elevated temperatures, thereby enhancing the densification of materials. Three distinct trials (1–3) with varying parameters, including compaction pressure (350 MPa, 450 MPa, and 550 MPa), temperature (470 °C, 490 °C, and 510 °C), and soaking time (1.5 h, 2 h, and 2.5 h), significantly influenced the evolution of microstructure, densification behaviour, and mechanical properties. The compaction pressure was selected in such a manner that it would allow resettlement of the particles without cracks. The sintering temperature was maintained such that it was close to the best diffusion regime to facilitate the development of the necks without coarsening or melting of grains. The soaking time was set in a way that there was even heat penetration and full consolidation without thermal distortion. The process schematic of the entire process and property evaluation is given in Fig. 1.

The compacted billets were then placed in a vacuum furnace, and to prevent oxidation and burning, 5lit/min of CO_2 and SF_6 were allowed to enter into the furnace, and sintering was carried out at different temperature intervals with varying soaking time (1.5 h, 2 h and 2.5 h) to reduce defects, leading to improved structural integrity and performance of the magnesium composites, as inferred in Table 2. Initially, it was determined to establish the sintering temperature at 470 °C, a value significantly lower than the melting point. This choice postulates the process that remains within the solid-state sintering region, thereby preventing the collapse of the compact's structure, as well as the melting and oxidation of magnesium. Then the temperature was further increased to 490 °C and 510 °C in order to improve interparticle debonding, reduce porosity and overall densification of synthesised hybrid composites. In conjunction with temperature variations, the soaking duration was adjusted since an increase in temperature facilitates faster diffusion and more mobile grain boundaries. Extended soaking times allow atoms more space to rearrange, resulting in a more uniform microstructure that optimises grain refinement, matrix-reinforcement bonding, and porosity reduction, while maintaining the thermal stability of

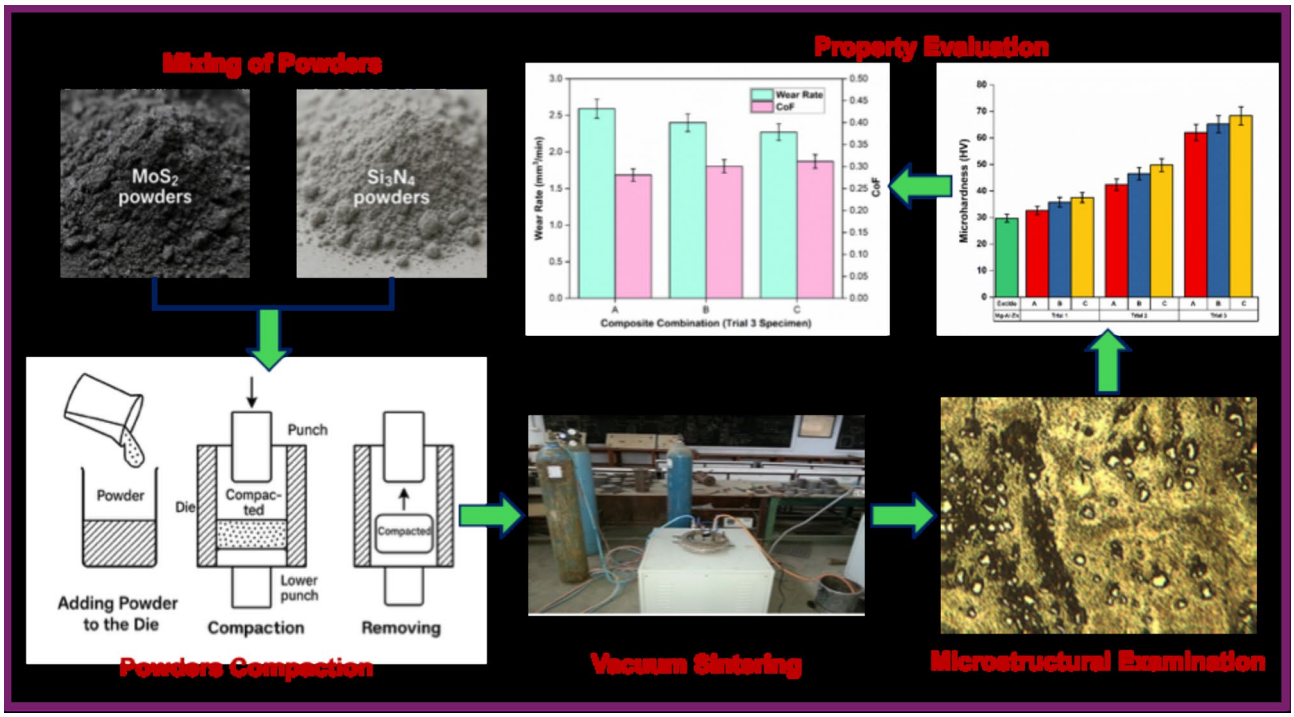

Fig. 1. Process schematic of the entire process and property evaluation.

S. No.	Combinations	Entitle/ samples		Compaction pressure (MPa)	Sintering temperature (°C)	Soaking time (h)
1	Mg–Al–Zn alloy	Base alloy		350	450	1.5
2	Mg–Al–Zn alloy + 2 wt% Si_3N_4 + 2 wt% MoS_2	Trial 1	A	350	470	1.5
3	Mg–Al–Zn alloy + 4 wt% Si_3N_4 + 2 wt% MoS_2		B	350	470	1.5
4	Mg–Al–Zn alloy + 6 wt% Si_3N_4 + 2 wt% MoS_2		C	350	470	1.5
5	Mg–Al–Zn alloy + 2 wt% Si_3N_4 + 2 wt% MoS_2	Trial 2	A	450	490	2
6	Mg–Al–Zn alloy + 4 wt% Si_3N_4 + 2 wt% MoS_2		B	450	490	2
7	Mg–Al–Zn alloy + 6 wt% Si_3N_4 + 2 wt% MoS_2		C	450	490	2
8	Mg–Al–Zn alloy + 2 wt% Si_3N_4 + 2 wt% MoS_2	Trial 3	A	550	510	2.5
9	Mg–Al–Zn alloy + 4 wt% Si_3N_4 + 2 wt% MoS_2		B	550	510	2.5
10	Mg–Al–Zn alloy + 6 wt% Si_3N_4 + 2 wt% MoS_2		C	550	510	2.5

Table 2. Sintering conditions of Si_3N_4-MoS_2 reinforced Mg–Al–Zn alloy.

the reinforcement phases and preventing undesirable intermetallic formation. Subsequently, the sintered sample was permitted to cool within the furnace under an inert atmospheric condition to prevent oxidation and to avert the formation of MgO layers, which might affect surface quality and mechanical properties.

Performance measures and experimental design for wear optimization

Compact specimens were meticulously sectioned from sintered billets utilising a low-speed diamond saw, followed by grinding and polishing to eliminate any surface irregularities. The composites' mechanical properties were tested according to the appropriate ASTM standards. The Archimedes method was used to measure density, and the ASTM E384 was used to measure Vickers microhardness. The average value was based on several indentations made on the polished surface. The compressive strength test according to ASTM E9.The wear analysis in the present study is conducted based on the Taguchi method with an L9 orthogonal array due to its effectiveness in evaluating multiple process parameters with a reduced number of experimental runs. In this case, three key factors, such as applied load, sliding velocity, and sliding distance, were each analysed at three different levels. A full factorial design would require 27 experiments (3^3), whereas the L9 design reduces it to 9 experiments without significantly compromising statistical accuracy. This not only minimizes experimental effort and resource consumption but also ensures robust optimization of wear behaviour under controlled variable interactions.

Results and discussion

An optical microscope was used to examine the microstructure observations of Mg–Al–Zn/Si_3N_4/MoS_2 alloy hybrid intermixture (Trial 1–3) with Picral as an etching medium as inferred in Fig. 2. The microstructure shows that the Si_3N_4/MoS_2 particles agglomerate in certain regions at trials 1,2 (a–c), implying that at lower compaction pressures, temperatures, and soaking intervals, molecules on powder particles' surfaces may not have enough surface energy to overcome activation barriers and migrate onto adjacent particles to form strong interactions. This entails a void region in the microstructure that leads to inadequate densification. Since particle forces may not be strong enough to overcome repulsive forces and hold particles together at low sintering temperatures. Hence, sintering parameters such as temperature, soaking time, and compaction pressure are increased for trial 3 (a–c). At higher processing parameters, it reduces porosity and improves interparticle bonding, causing denser microstructures and making the material reach equilibrium. This exhibits a refined grain structure, and the presence of Si_3N_4/ MoS_2 particles acts as nucleation sites for grain refinement during sintering, which impedes the movement of dislocations, enhancing the material's resistance to deformation, interfacial bonding, load transfer mechanisms, and mechanical properties of the synthesised hybrid immixture.

SEM was used to analyse the dispersion morphology, agglomeration, particle bonding, porosity, voids, and microcracks of the synthesised hybrid intermixture as illustrated in Fig. 3a. Trial A exhibited particle agglomeration due to insufficient compaction pressure, sintering temperature, and soaking duration. This is attributable to the fact that these parameters restrict the contact area between particles, which is crucial for commencing diffusion during sintering. Under these circumstances, fine particles such as MoS_2 tend to aggregate due to weak Van der Waals forces and are not efficiently dispersed into the matrix. It was also observed that the soaking duration during sintering facilitates the necessary time for diffusion, pore closure, and particle coalescence. If the duration is insufficient, the sintering process remains incomplete, resulting in isolated clusters of particles that fail to integrate entirely into the matrix, which is regarded as a primary factor contributing to the clustering of strengthening particles in the base alloy. In contrast, an increase in these parameters Fig. 3b and Fig. 3c results in tighter particle packing and increased green density, leading to enhanced contact between particles, which improves interparticle bonding during the sintering process. Improving sintering temperatures and soaking time increases the thermal energy required to initiate atomic diffusion processes, thus facilitating solid-state bonding. This leads to enhanced densification, improved mechanical properties, and a more consistent microstructure.

The XRDA analysis was utilised to provide quantitative data concerning the phase distribution in the composite material. Comprehending the effective reinforcement offered by Si_3N_4 and MoS_2 within the Mg–Al–Zn matrix is essential, as the distribution and amount of the reinforcement phase play a significant role in determining

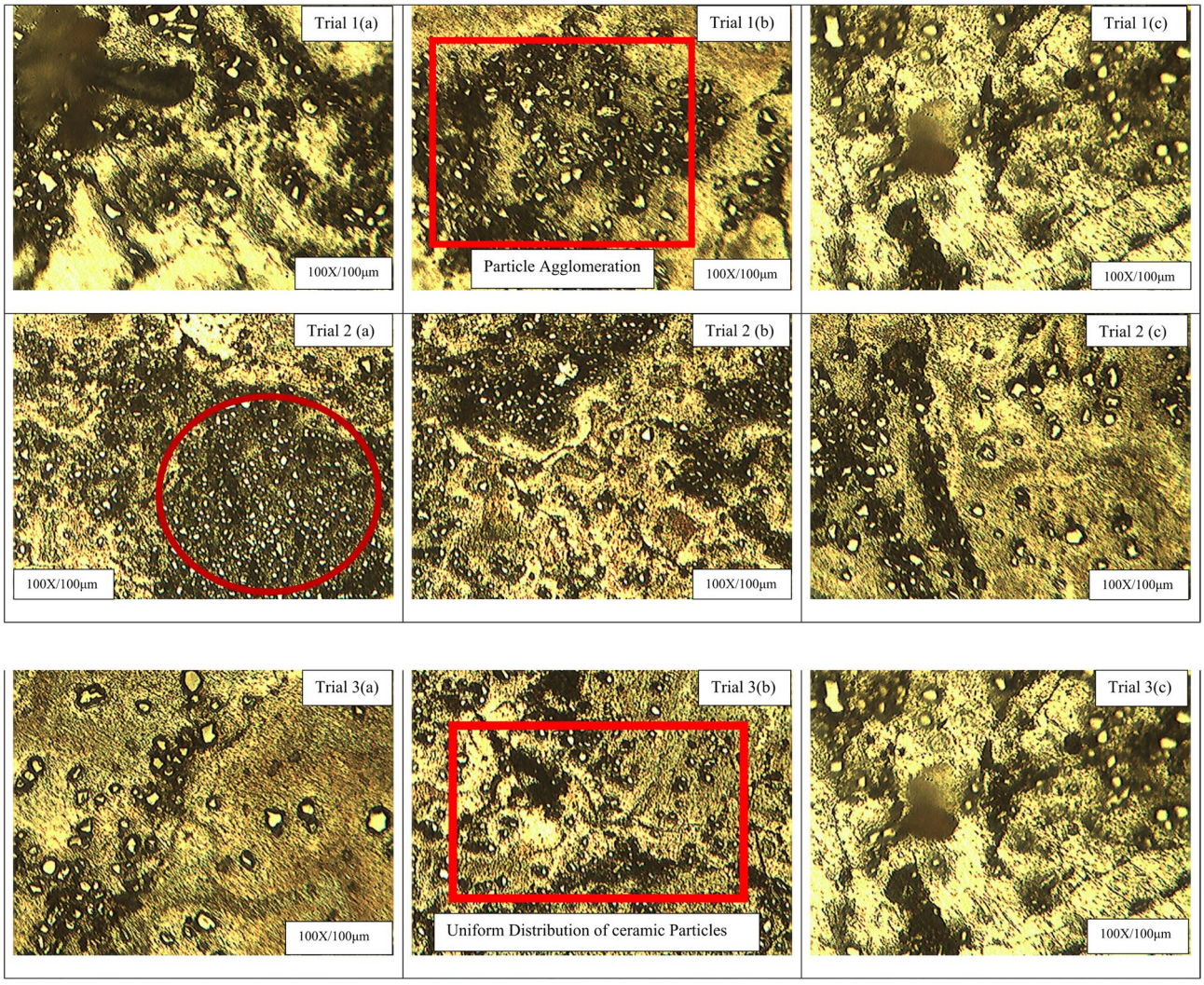

Fig. 2. (Trial 1–3) Microstructure of Si_3N_4/MoS_2/Mg–Al–Zn alloy composites showing particle distribution and agglomeration.

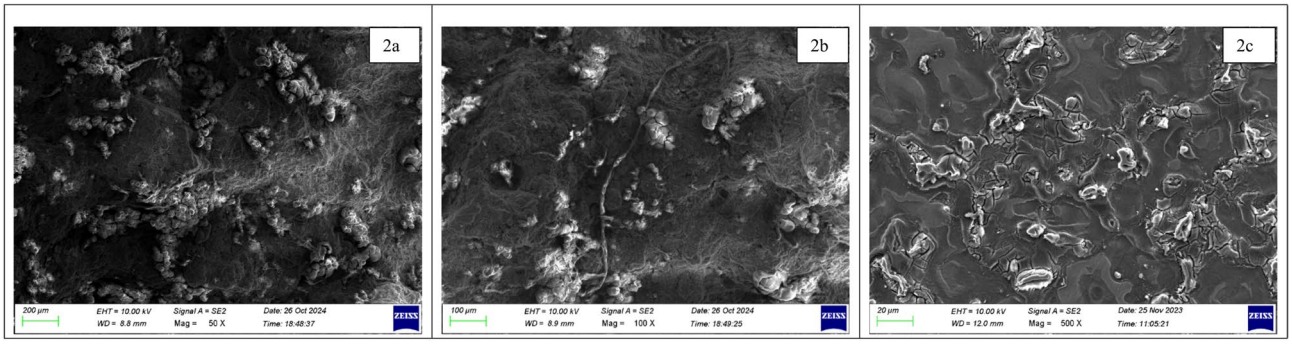

Fig. 3. (**a**–**c**) SEM image of Si_3N_4/MoS_2/Mg–Al–Zn alloy composites showing the reinforcement particles.

the final characteristics of the composite material. It was noted that Si_3N_4/MoS_2/Mg–Al–Zn interphases, which include Mg_2Si, AlN, MgS, and Zn–Al intermetallics, may form due to diffusion and chemical reactions that take place during the sintering process. The interphases significantly impact mechanical performance, especially in terms of bonding, strength, and wear resistance. The reinforcements exhibit chemical stability under controlled sintering conditions and are unlikely to react significantly with the matrix. This leads to clean interfaces devoid of compound formation, permitting the observation of only the parent phases (Mg, Al, Zn, Si_3N_4, MoS_2) in

XRDA. Hence, it confirms the peaks of synthesized composites of Mg (100), Al (111). Zn (002), Si_3N_4 (110), MoS_2 (103) at different 2θ values[18] as inferred in Fig. 4. It implies that during the powder metallurgy process, sintering temperatures generally remain beneath the melting point of the base materials. This circumstance minimises the potential for substantial diffusion at the particle interfaces, allowing the alloying element to largely retain its original phase.

Density and hardness

The density of the hybrid intermixture was investigated using Archimedes' principle by measuring it in air with apparent mass when immersed in a liquid, as illustrated in Eq. (1)[3].

$$\rho_{\text{hybrid composite}} = \frac{\text{Mair}}{\text{V}} \tag{1}$$

Observation shows that the density of sintered composites improved slightly for all the trials compared to the Mg–Al–Zn alloy. This suggests that increasing the weight% of Si_3N_4 increases the proportion of the denser material in the composite by occupying more volume relative to the lighter matrix, as shown in Fig. 5a. Further, the ceramic reinforcement Si_3N_4 has a density of 3.2 g/cm^3, while MoS_2 has a density of 5.06 g/cm^3, both of which exceed the density of the Mg–Al–Zn alloy at 1.8 g/cm^3. Incorporating these denser particles into the lighter alloy matrix also contributes to enhancing the overall density of the composite. While sintering, Si_3N_4 and MoS_2 particles it suppress grain development in the matrix material. This inhibition can result in a firmer microstructure with more grain boundaries, resulting in smaller voids between grains and elevated density. Further, a disparity in thermal expansion coefficients between the matrix and ceramic particles may cause internal stresses during cooling after sintering, leading to higher densification.

The Microhardness of synthesized hybrid intermixtures was analysed as per ASTM E384-17. It was found that a low sintering temperature, compaction pressure, and soaking time resulted in reduced hardness for trials 1 (23.21%) and 2 (50.41%), attributed to inadequate wettability, which hinders grain development among intermixtures and weakens grain boundaries, illustrated in Fig. 5b. It was also noted that the reduction in such processing can lead to the formation of pores that act as stress concentrators, weakening the material and reducing its hardness. By increasing its processing parameters, the hardness of such composites was increased to 78.80% due to improved temperatures, which promote greater particle mobility, allowing particles to rearrange and pack more closely together. The porosity is further reduced by the increase in compaction pressure, which squeezes the powder particles closer together and promotes stronger metallurgical bonds during sintering. Additionally, by increasing the sintering temperature and soaking time, it allows more time for atoms to diffuse across particle boundaries, resulting in stronger inter-particle bonds between the intermixture, resulting in higher hardness of the hybrid intermixture.

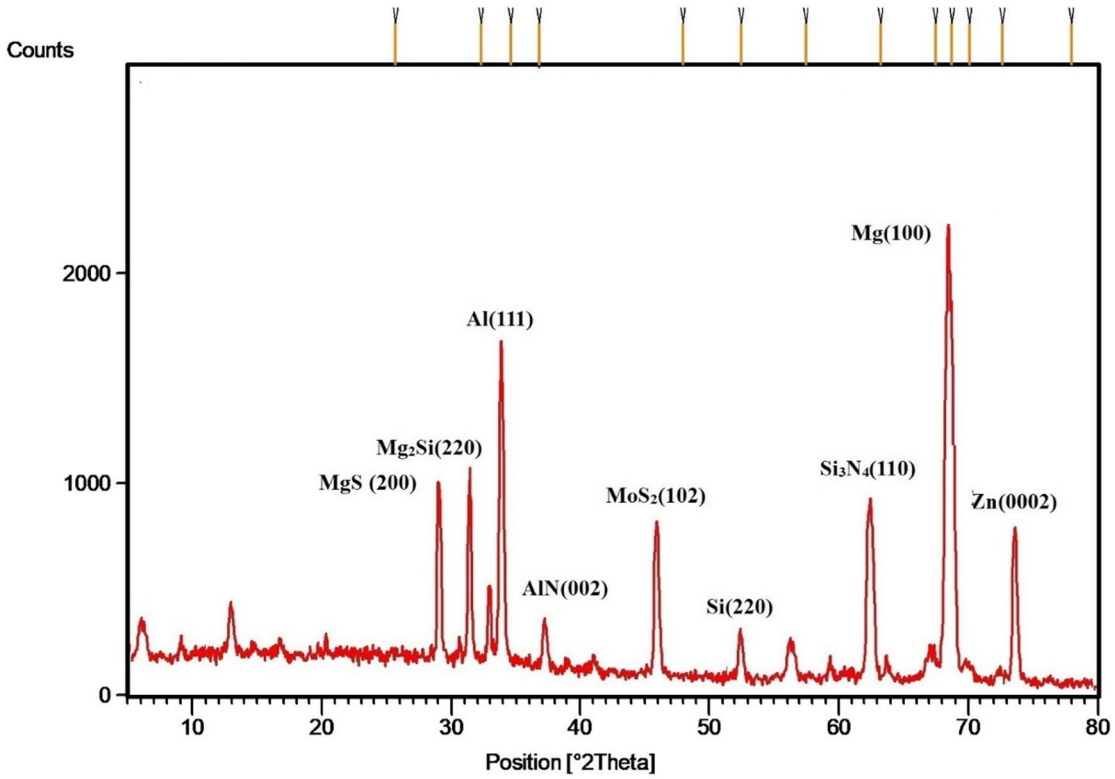

Fig. 4. XRD analysis of Si_3N_4/MoS_2/Mg–Al–Zn alloy composites showing peaks of reinforcing particles.

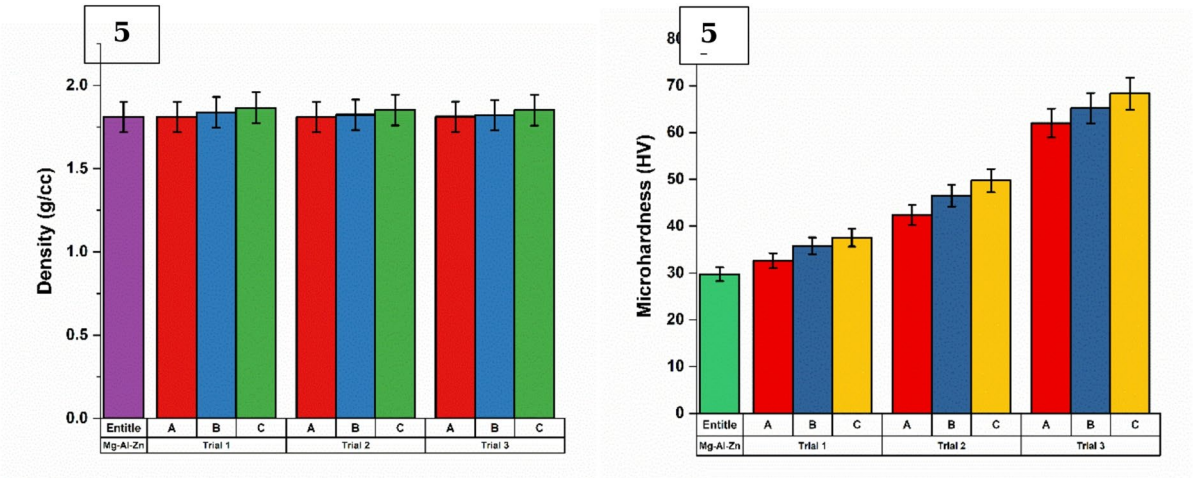

Fig. 5. (**a**,**b**) Density and microhardness of Si_3N_4/MoS_2/Mg–Al–Zn alloy composites of different trials comparing with the base alloy.

Compressive strength

The compressive strength of sintered hybrid composites was evaluated in accordance with ASTM E9 standards at room temperature. It was inferred that for all combinations and it exhibited a proportional increase when compared to the base alloy. Trial 3 (63.44%) exhibits higher compressive strength, whereas trials 2 (51.94%) and 1 (38.33%) have lower compressive strength because they may not allow enough time for stress to relieve at lower temperatures, resulting in residual stresses that weaken composites[19]. It was also observed that the improper sintering may induce phase transitions and result in an inferior microstructure that indicates minimised mechanical properties during the sintering of magnesium composites. Conversely, increasing such a process parameter elevates particle padding, resulting in a more coherent microstructure, mitigates particle debonding, and propels the material's resistance to compressive forces, as shown in Fig. 6. It was also found that longer soaking time (2.5 h) of hybrid intermixture increases bonding at the reinforcement-matrix interface, minimising microcracks and increasing load transfer during compression. Additionally, it aids in lowering porosity by enabling trapped gases to escape and densifying the material, increasing its resistance to compressive stresses.

Corrosion

Mg-Al-Zn alloys often contain intermetallic phases, such as $Mg_{17}Al_{12}$ and $MgZn_2$, which are more anodic and it can initiate localized corrosion and minimize corrosion resistance. The incorporation of Si_3N_4/MoS_2 particles serves as barriers at Mg particle surfaces, obstructing direct contact and diffusion between Mg alloying elements by inhibiting the nucleation and formation of intermetallic phases at grain boundaries. This improves grain refining during sintering and obtains a higher density of grain boundaries from smaller grain sizes, which effectively expands the number of prospective sites for corrosion detention, improving the material's overall resistance to corrosion, as inferred in Fig. 7. The corrosion resistance at both lower and higher sintering levels increases, as lower temperatures limit grain formation, resulting in a more refined microstructure that enhances the material's resistance to localised corrosion[20]. Higher sintering temperatures result in a denser microstructure owing to particle diffusion, and enhanced bonding can improve resistance by reducing the gaps that allow corrosive agents to penetrate the material.

Wear analysis

The wear behaviour of Si_3N_4/MoS_2/Mg–Al–Zn composites enhances with increasing density, hardness, compressive strength, and corrosion resistance, since these attributes jointly increase the material's load-bearing capacity, surface integrity, and damage resistance during sliding. Vacuum sintering processing enhances densification, which decreases porosity and improves load distribution under sliding conditions. Reduced porosity decreases stress concentration points that commonly serve as sites for crack initiation, thus improving wear resistance. With increasing density, the composite achieves greater structural compactness, facilitating improved mechanical interaction between the matrix and the reinforcements. This directly enhances hardness, a crucial property influencing resistance to surface deformation and micro-abrasion. The Si_3N_4 particles enhance the matrix's strength, whereas the lubricating properties of MoS_2 decrease friction, resulting in a reduced wear rate. The improved compressive strength reinforces the material's capacity to withstand higher normal loads without experiencing surface failure, particularly in high-pressure sliding circumstances. A denser, stronger composite can withstand plastic flow and micro fracturing, which are prevalent wear processes in softer metals. In addition, the composite's corrosion resistance is enhanced by the passive nature of Al and the inertness of ceramic reinforcements, which are critical in tribocorrosion environments. Corrosion-induced degradation frequently results in increased wear; however, enhanced corrosion resistance maintains surface integrity, thus ensuring low wear rates over time. Increased density indicates the effectiveness of vacuum sintering in

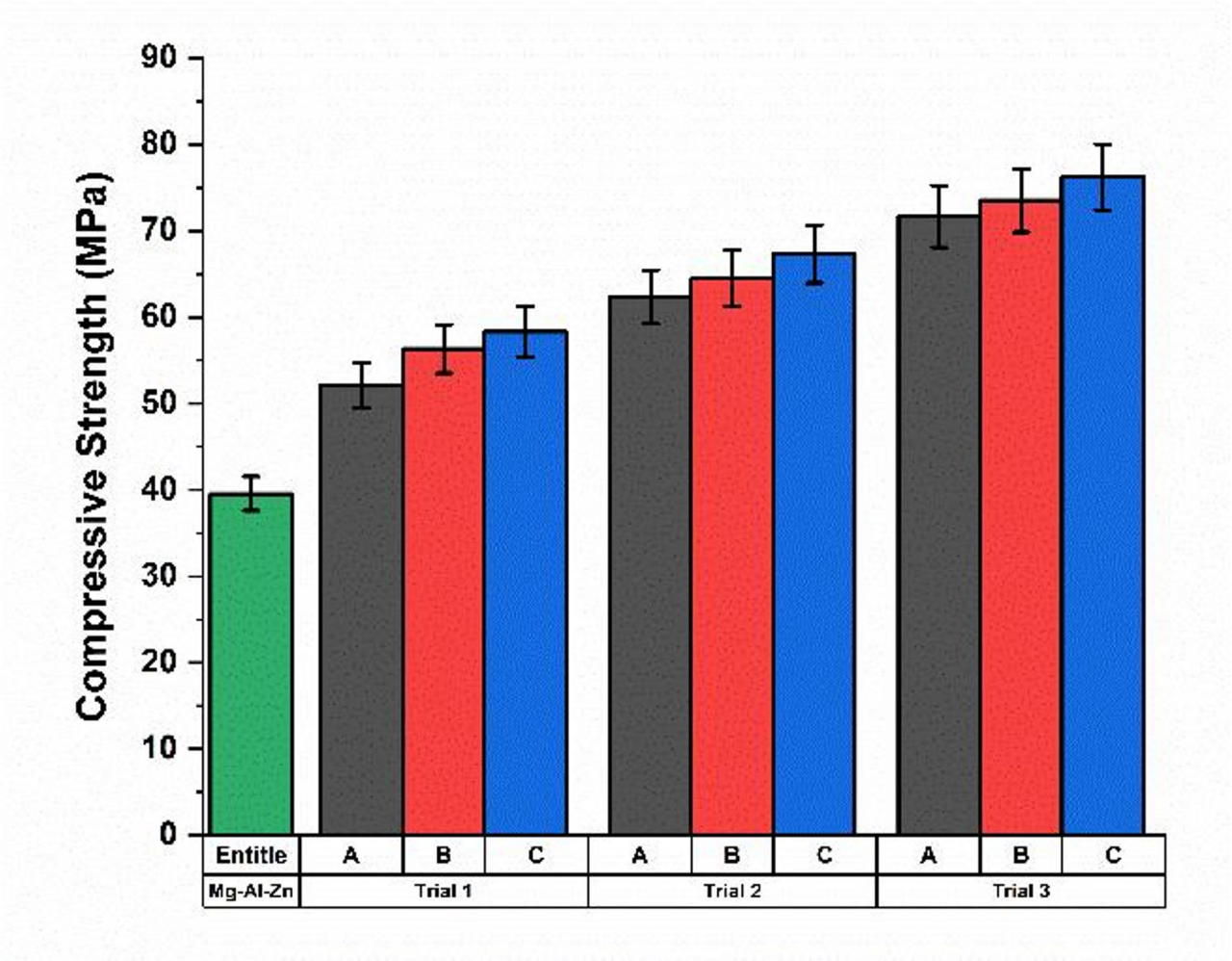

Fig. 6. Compressive strength of Si_3N_4/MoS_2/Mg–Al–Zn alloy composites of different trials comparing with the base alloy.

consolidating the hybrid composite and supports improvements in hardness, strength, and corrosion resistance, which collectively enhance wear performance across various operating conditions.

Through the examination of various characterisations, it was determined that trial 3 exhibits a significant characteristic due to improved sintering parameters. Consequently, it was decided to conduct a wear test for the same combinations of varying input parameters using a pin-on-disc wear apparatus to assess the wear resistance of synthesised magnesium composites.

Preliminary wear performance of hybrid composites without statistical optimization

Before performing optimization through Taguchi's orthogonal array, wear rate and coefficient of friction (CoF) for the hybrid composites were measured independently. These results provide insight into the base tribological behaviour of the composites under consistent trial 3 conditions, without influence from optimization algorithms. Figure 8 shows the wear rate and CoF across different composite combinations (A, B, C).

It was observed that the composite with 6 wt% Si_3N_4 + 2 wt% MoS_2 (Combination C) exhibited the lowest wear rate (2.27 mm^3/min), illustrating a superior resistance to material loss. This performance is attributed to the higher ceramic reinforcement, which provides enhanced hardness and structural integrity under sliding contact. In contrast, Combination A with 2 wt% Si_3N_4 recorded the lowest CoF (0.2807), likely due to reduced abrasive interactions and effective lubrication from MoS_2. The noted enhancement in wear behaviour clearly indicates the enhanced microstructural integrity attained through optimised processing conditions.

From the above results in Table 3, it is evident that increasing the Si_3N_4 content improves wear resistance, as reflected in the decreasing wear rate from Combination A to C. It was also noted that enhanced densification improves the load-bearing capacity of the composite, whereas consistent particle-matrix bonding aids in preventing material loss during sliding. Si_3N_4 enhances wear resistance through hard-particle reinforcement and load transfer, while MoS_2 mitigates abrasive and adhesive wear by creating a solid-lubricant film. However, a trade-off is observed in terms of CoF, which increases slightly with ceramic content due to increased surface roughness and contact area. These findings highlight the intrinsic tribological behaviour of the composites

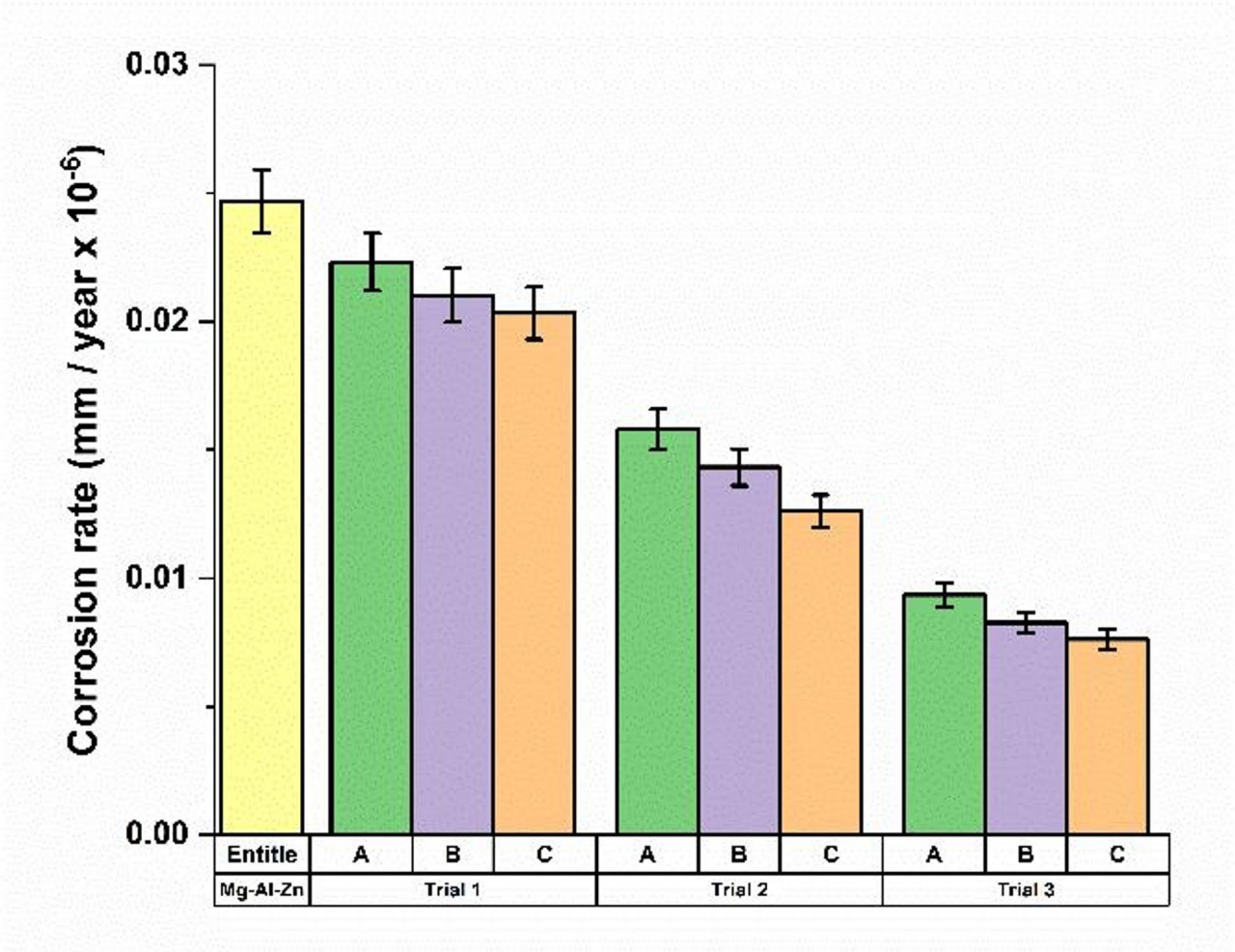

Fig. 7. Corrosion resistance of Si_3N_4/MoS_2/Mg–Al–Zn alloy composites of different trials comparing with the base alloy.

before statistical optimization, and form the basis for further Taguchi-based refinement. Figure 9 shows the SEM image of the worn-out surface of the prepared composite material after conducting the wear study.

Wear performance of hybrid composites with statistical optimization

Experiments are conducted as per Taguchi's L9 orthogonal array of experimentation (Table 4) with Trial 3 composites to find out the best optimal combination of parameters to obtain a lower wear rate and reduced coefficient of friction (CoF)[21]. All the input parameters (combinations, applied load, sliding velocity, sliding distance) are varied at three different levels based on the equipment's specifications to find out the mean of the responses based on the main effects plot. The statistical significance of the chosen material is found using the ANOVA. The mathematical model in the form of regression equations is obtained to assess the experimental results for the optimal wear characteristics (wear rate and CoF).

The mean response table for wear rate and CoF of Trial 3 composites are given in Table 5. From the table, it is clear that applied load contributes more to deciding the wear rate and CoF of the prepared composites, followed by the composite type, sliding velocity and sliding distance. For the wear parameters to be obtained, theoretically, sliding velocity contributes more when compared to the sliding distance. In CoF determination, there is a very minimal difference in the delta values obtained. Hence, the order of contribution in deciding the wear rate and CoF is kept as applied load, followed by the composite type, sliding velocity and sliding distance. According to Archard's law, the change in wear rate on the specimens is proportionate to the amount of load on the wear surface. Increased stress and increased contact time on the wear surface increases the wear loss of the prepared specimen. More contact pressure at the interface of the sliding surface with the wear test specimen increases the temperature, which in turn increases the wear rate on the test specimen. From the table, it is clear that the third combination of the prepared specimen (Mg–Al–Zn alloy + 6 wt% Si_3N_4 + 2 wt% MoS_2), applied load at 10 N, sliding velocity at 0.5 ms^{-1} and sliding distance at 500 m are the optimal parameter for minimal wear rate on the Trial 3 specimen. Similarly, for CoF, the first combination of the prepared specimen (Mg–Al–Zn alloy + 2 wt% Si_3N_4 + 2 wt% MoS_2), applied load at 10 N, sliding velocity at 1 ms^{-1}, and sliding distance at 1500

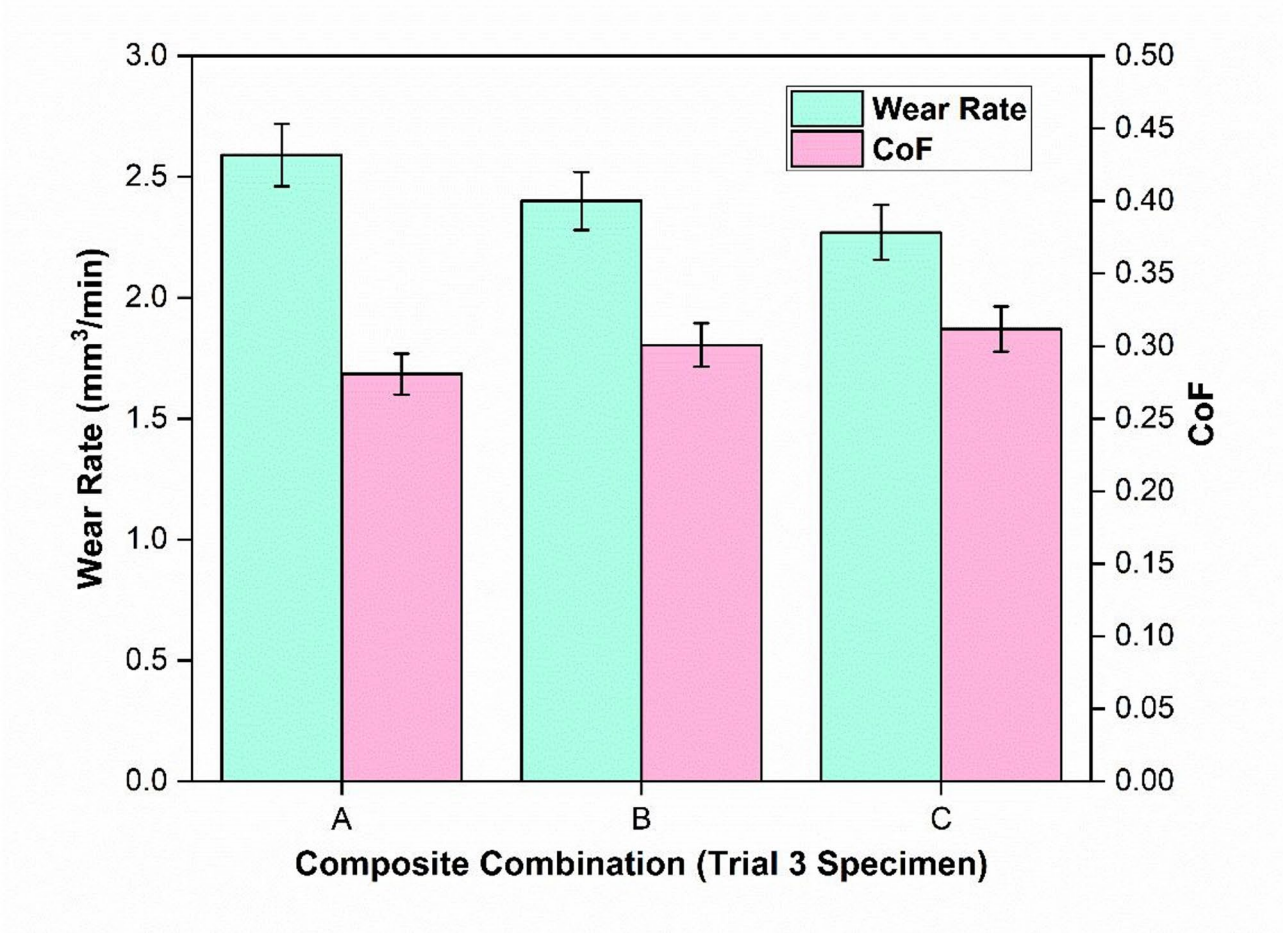

Fig. 8. Wear performance (wear rate and CoF) across different composite combinations (**A**–**C**).

Composite combination	Wear rate (mm^3/m)	Coefficient of friction (CoF)
Mg-Al-Zn alloy (2% Si_3N_4 + 2% MoS_2) - A	2.59	0.2807
Mg-Al-Zn alloy (4% Si_3N_4 + 2% MoS_2) - B	2.40	0.3007
Mg-Al-Zn alloy (6% Si_3N_4 + 2% MoS_2) - C	2.27	0.3117

Table 3. Average wear rate and CoF for composites A, B, and C (Trial 3 conditions).

m are the optimal parameters. The reason for the lower CoF is due to the lesser Si_3N_4 (2%) percentage added to the composite and the increased sliding velocity (1 m/s). This reduces the friction generated between the wear specimen and its counterpart during the wear examination[22].

The mean response plot given in Fig. 10 depicts the increase in the wear rate of the Trial 3 specimen as the applied load increases from 10 N to 30 N. This shows that a lower applied load has a significant contribution in deciding the wear rate of the prepared composite. The lower the sliding velocity, the lower the wear rate. But in the plot shown below, though the optimal wear rate is obtained for the second level (0.5 m/s) sliding velocity, the margin of the value for it compared with lower sliding velocities is very low. Hence, the 0.5 m/s of sliding velocity has a positive influence on the wear rate. Sliding distance supports the results of applied load and sliding distance, with the optimal wear rate obtained at a lower sliding distance of 500 m. All these optimal results are obtained for the third combination of composites (Mg-Al-Zn alloy + 6 wt% Si_3N_4 + 2 wt% MoS_2) prepared at trial 3 conditions. A similar trend of applied load for the optimal CoF is given in Fig. 11. Higher levels of sliding velocity (1 m/s) and sliding distance (1500 m) contribute to the optimal CoF for the first combination (Mg–Al–Zn alloy + 2 wt% Si_3N_4 + 2 wt% MoS_2) of the prepared specimens at trial 3 conditions. As the sliding velocity and sliding distance increase, the friction and heat generation would be lesser between the friction surfaces for the specimen with a lesser Si_3N_4 (2%) percentage. This results in the desired CoF (lower). The plots and their trends look clear and consistent in the influence of factors in both the response variables for the specimens prepared at Trial 3 working conditions.

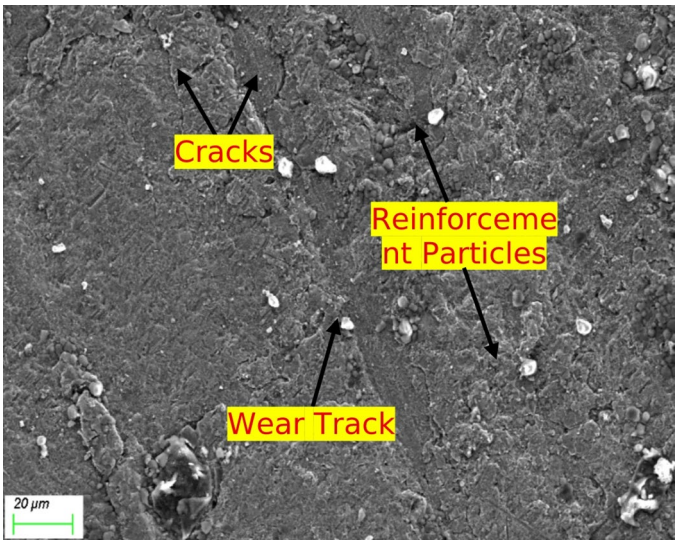

Fig. 9. SEM image showing the cracks, wear track and the reinforcement particles after wear study.

S. No.	Combinations	Applied load (*N*)	Sliding velocity (m/s)	Sliding distance (m)	Wear rate (mm^3/m)	CoF
1	Mg–Al–Zn alloy + 2 wt% Si_3N_4 + 2 wt% MoS_2	10	0.25	500	1.82	0.159
2	Mg–Al–Zn alloy + 2 wt% Si_3N_4 + 2 wt% MoS_2	20	0.5	1000	2.62	0.231
3	Mg–Al–Zn alloy + 2 wt% Si_3N_4 + 2 wt% MoS_2	30	1	1500	3.33	0.452
4	Mg–Al–Zn alloy + 4 wt% Si_3N_4 + 2 wt% MoS_2	10	0.5	1500	1.71	0.167
5	Mg–Al–Zn alloy + 4 wt% Si_3N_4 + 2 wt% MoS_2	20	1	500	2.53	0.246
6	Mg–Al–Zn alloy + 4 wt% Si_3N_4 + 2 wt% MoS_2	30	0.25	1000	2.96	0.489
7	Mg–Al–Zn alloy + 6 wt% Si_3N_4 + 2 wt% MoS_2	10	1	1000	1.62	0.172
8	Mg–Al–Zn alloy + 6 wt% Si_3N_4 + 2 wt% MoS_2	20	0.25	1500	2.42	0.255
9	Mg–Al–Zn alloy + 6 wt% Si_3N_4 + 2 wt% MoS_2	30	0.5	500	2.76	0.508

Table 4. Experimental response for wear performance (wear rate and CoF).

Response	Level	Combinations	Applied load (*N*)	Sliding velocity (m/s)	Sliding distance (m)
Wear rate (mm^3/m)	1	2.590	1.717*	2.400	2.370*
	2	2.400	2.523	2.363*	2.400
	3	2.267*	3.017	2.493	2.487
	Delta	0.323	1.300	0.130	0.117
	Rank	2	1	3	4
CoF	1	0.2807*	0.1660*	0.3010	0.3043
	2	0.3007	0.2440	0.3020	0.2973
	3	0.3117	0.4830	0.2900*	0.2913*
	Delta	0.0310	0.3170	0.0120	0.0130
	Rank	2	1	4	3

Table 5. Mean response table for wear performance (wear rate and CoF). *Optimal level.

Regression analysis is one of the statistical methods used to find out the relationship between the input and output process parameters. Equations (2) and (3) are used to find out the wear rate and CoF on the prepared specimens. The objective of using the obtained regression equation is to achieve a minimum wear rate and CoF for any composite materials without the conduct of experimentation. This gives the association of various control parameters that contribute to the lowest wear rate and CoF.

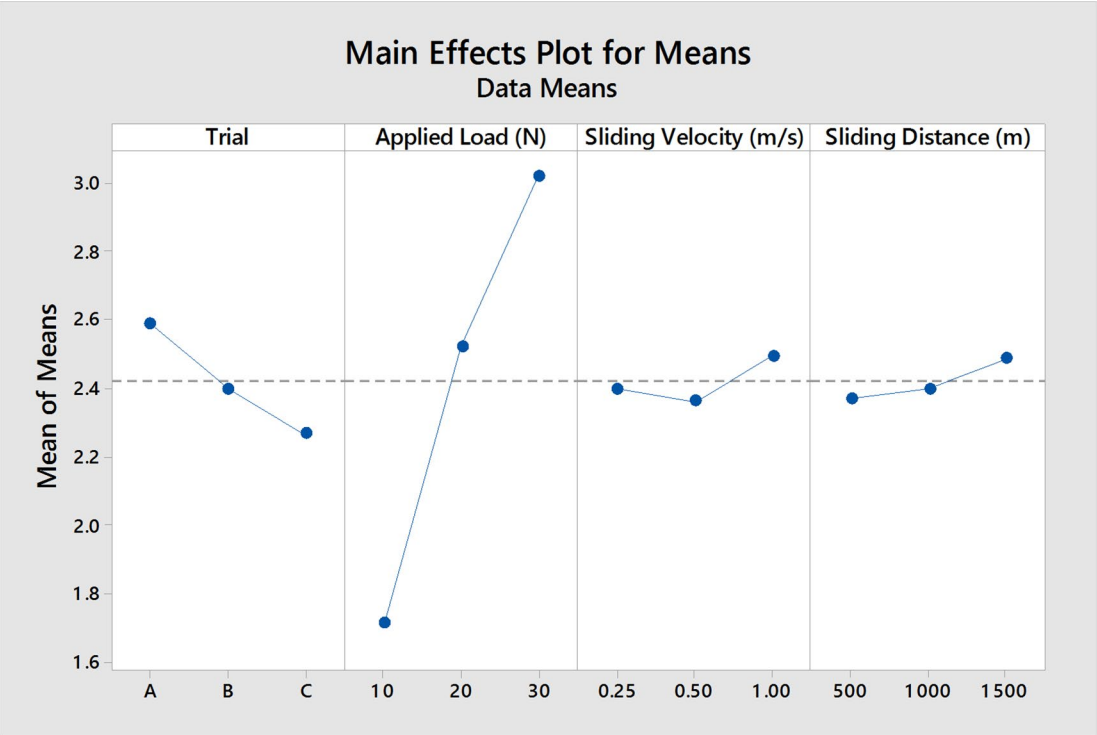

Fig. 10. Mean response plot for Wear Rate with four different varying input parameters at three different levels.

Fig. 11. Mean response plot for CoF with four different varying input parameters at three different levels.

Sources	DF	Adj SS	Adj MS	F-Value	*P*-Value	% contribution
	Wear rate (mm^3/m)					
Applied load (N)	2	2.58409	1.29204	16.31	0.058	92.57%
Sliding velocity (m/s)	2	0.02696	0.01348	0.17	0.855	0.96%
Sliding distance (m)	2	0.02202	0.01101	0.14	0.878	0.78%
Error	2	0.15842	0.07921			5.67%
Total	8	2.79149				100%
Sources	CoF					
Applied load (N)	2	0.163694	0.081847	110.45	0.009	98.79%
Sliding velocity (m/s)	2	0.000266	0.000133	0.18	0.848	0.16%
Sliding distance (m)	2	0.000254	0.000127	0.17	0.854	0.15%
Error	2	0.001482	0.000741			0.89%
Total	8	0.165696				100%

Table 6. ANOVA results showing the significance of process parameters on wear rate and coefficient of Friction.

Response	S	*R*-sq	*R*-sq (adj)
Wear rate (mm^3/m)	0.281445	94.32%	77.30%
CoF	0.027221	99.11%	96.42%

Table 7. Mean summary of ANOVA for wear performance (wear rate and CoF).

$$\begin{aligned}\text{WearRate}\left(\text{mm}^3/\text{m}\right) = \; & 2.4189 - 0.702\ \text{Applied Load (N)\_10} + 0.104\ \text{Applied Load (N)\_20} \\ & + 0.598\ \text{Applied Load (N)\_30} - 0.019\ \text{Sliding Velocity (m/s)\_0.25} \\ & - 0.056\ \text{Sliding Velocity (m/s)\_0.50} + 0.074\ \text{Sliding Velocity (m/s)\_1.00} \\ & - 0.049\ \text{Sliding Distance (m)\_500} - 0.019\ \text{Sliding Distance (m)\_1000} \\ & + 0.068\ \text{Sliding Distance (m)\_1500}\end{aligned} \tag{2}$$

$$\begin{aligned}\text{CoF} = \; & 0.29767 - 0.1317\ \text{Applied Load (N)\_10} - 0.0537\ \text{Applied Load (N)\_20} \\ & + 0.1853\ \text{Applied Load (N)\_30} + 0.0033\ \text{Sliding Velocity (m/s)\_0.25} \\ & + 0.0043\ \text{Sliding Velocity (m/s)\_0.50} - 0.0077\ \text{Sliding Velocity (m/s)\_1.00} \\ & + 0.0067\ \text{Sliding Distance (m)\_500} - 0.0003\ \text{Sliding Distance (m)\_1000} \\ & - 0.0063\ \text{Sliding Distance (m)\_1500}\end{aligned} \tag{3}$$

The ANOVA of wear rate and CoF of Trial 3 specimens are reported in Table 6. The applied load was found to be the most influential factor affecting both wear rate and CoF, with percentage contributions of 92.57% and 98.79%, respectively. This is supported by the high F-values (16.31 for wear rate and 110.45 for CoF) and low p-values (0.058 and 0.009). The p-value for CoF is less than 0.05, indicating high statistical significance at a 95% confidence level. The p-value for wear rate is slightly above the conventional 0.05 threshold but still indicates a strong trend toward significance, especially given the small sample size and low residual error (5.67%). These results highlight that applied load is a statistically significant predictor for both tribological responses, while sliding speed and sliding distance have minor effects, as their p-values are much greater than 0.05. This falls within the 95% confidence limits chosen for the present experimental study.

Sliding velocity and sliding distance, on the other hand, contribute less than 1% each in both responses, and their p-values ($>>0.05$) show that they are statistically insignificant within the test conditions used. These results confirm that optimising applied load is critical in achieving minimal wear rate and friction in the hybrid composites.

Table 7 gives the details of R-Sq values of wear rate and CoF of Trial 3 specimens with 94.32% and 99.11%, respectively. Based on the R-Sq values it is evident that the parameters chosen for the present experimentation of wear analysis for specimens prepared through Trial 3 conditions are accurate and correct. The same experimental conditions and procedures can be utilised for similar kinds of experimentation to be conducted in future. Based on the tabulated results, it is clear that the results predicted through this model are accurate and can have complete reliability. A higher R-squared value indicates that the independent variables in the model explain a large percentage of the variance seen in the dependent variable. This means the model is more precise and reliable in predicting the dependent variable with the given independent variables[23].

Based on the experiments conducted and analysis of results, the best optimal parametric level to attain minimal Wear rate is at a composite combination of Mg–Al–Zn alloy + 6 wt% Si_3N_4 + 2 wt% MoS_2, applied load at 10 N, sliding velocity at 0.5 ms^{-1} and sliding distance at 500 m on the Trial 3 specimen and for minimal CoF is at a composite combination of Mg–Al–Zn alloy + 2 wt% Si_3N_4 + 2 wt% MoS_2, applied load at 10 N, sliding velocity at 1 ms^{-1}, and sliding distance at 1500 m, respectively.

Conclusions

This study achieved an effective production of Si_3N_4/MoS_2 reinforced Mg–Al–Zn alloy composites through the vacuum sintering method. The process involved varying sintering temperature, compaction pressure, and soaking time across three weight proportion trials using a vacuum furnace, with the findings presented below. It was observed that an increase compaction pressure results in tighter particle packing and increased green density, leading to enhanced contact between particles, which improves interparticle bonding during the sintering process. Further improving sintering temperatures and soaking time increases the thermal energy required to initiate atomic diffusion processes, thus facilitating solid-state bonding. This leads to enhanced densification, improved mechanical properties, and a more consistent microstructure. The details of findings are listed below.

1. The microstructure shows that the Si_3N_4/MoS_2 particles agglomerate in certain regions at trial 1,2 (a–c), implying that at lower compaction pressures, temperatures, and soaking intervals, molecules on powder particles' surfaces may not have enough surface energy to overcome activation barriers and migrate onto adjacent particles to form strong interactions.
2. At higher processing parameters, it exhibits a refined grain structure, and the presence of Si_3N_4/MoS_2 particles acts as nucleation sites for grain refinement during sintering, which impedes the movement of dislocations enhancing the mechanical properties of synthesised hybrid immixture.
3. A difference in the thermal expansion coefficients of the matrix and ceramic particles can lead to internal stresses during the cooling phase post-sintering, resulting in a densification increase of up to $2.8 \pm 0.01\%$ when compared to the base alloy.
4. The hardness of hybrid composites was increased to $43.47 \pm 0.001\%$ due to higher temperatures which promote greater particle mobility, allowing particles to rearrange and pack more closely together.
5. A higher particle padding strengthens microstructure, reduces particle debonding, and propels compressive strength to maximum of $51.16 \pm 0.02\%$.
6. Si_3N_4/MoS_2 particles prevent direct contact and diffusion at alloy surfaces, improving grain refinement during sintering and grain boundary density from lower grain sizes and elevating corrosion detention sites to $30.86 \pm 0.01\%$.
7. The optimised parameters obtained through Taguchi analysis—particularly a composite formulation of Mg–Al–Zn alloy + 6 wt% Si_3N_4 + 2 wt% MoS_2, with an applied load of 10 N, sliding velocity of 0.5 m/s, and sliding distance of 500 m—demonstrate significant improvement in wear resistance. These findings have strong practical implications in high-performance sectors such as automotive braking systems, engine housings, and aerospace fasteners, where lightweight yet durable materials are essential with reduced material loss, longer service life, and improved reliability of components.

Data availability

The datasets used and/or analysed during the current study are available from the corresponding author on reasonable request.

Received: 9 December 2024; Accepted: 3 December 2025
Published online: 05 December 2025

References

1. Bocchini, G. F. Influence of process parameters on precision of PM parts. *Powder Metall.* **28**, 155–165 (1985).
2. Čapek, J. & Vojtěch, D. Effect of sintering conditions on the microstructural and mechanical characteristics of porous magnesium materials prepared by powder metallurgy. *Mater. Sci. Eng. C.* **35**, 21–28 (2014).
3. Zhao, Z., Zhang, T., Yang, Q., Li, M. & Li, J. Sintering and densification mechanism of SiC particle reinforced AZ91D magnesium matrix composite materials owing binder jetting. *Powder Technol.* **452**, 120609 (2025).
4. Sharma, S. K. et al. Significance of the powder metallurgy approach and its processing parameters on the mechanical behavior of magnesium-based materials. *Nanomaterials.* **15**, (2025).
5. Zhou, H. et al. Hot deformation behavior and dynamic recrystallization mechanism of Cr-Co-Ni particle-reinforced AZ31 magnesium matrix composite. *J. Alloys Compd.* **1022**, 179923 (2025).
6. Li, C. P., Li, Y. Q., Li, C. F., Chen, H. Y. & Ma, Y. L. Effect of SiC on microstructure and mechanical properties of Nano-SiC/Mg-8Al-1Sn composites. *J. Mater. Eng. Perform.* **34**, 3884–3893 (2025).
7. Ghasali, E., Alizadeh, M., Niazmand, M. & Ebadzadeh, T. Fabrication of magnesium-boron carbide metal matrix composite by powder metallurgy route: comparison between microwave and spark plasma sintering. *J. Alloys Compd.* **697**, 200–207 (2017).
8. Rai, A., Rai, P., Kumar, V., Singh, N. K. & Singh, V. K. Effect of sintering temperature on the Physico-Mechanical behavior of SiC reinforced Zinc-Magnesium based composite. *Met. Mater. Int.* **27**, 3164–3172 (2021).
9. Singh, N. K., Balaguru, S., Rathore, R. K., Namdeo, A. K. & Kaimkuriya, A. Multi-criteria decision-making technique for optimal material selection of AA7075/SiC composite foam using COPRAS technique. *J. Mines Metals Fuels.* **71**, 1374–1379 (2023).
10. Suneesh, E. & Sivapragash, M. Behaviour of micro- and nano-alumina-reinforced Mg–3Zn–0.7Zr–1Cu alloy composites processed at different sintering temperatures. *Rare Met.* **40**, 143–155 (2021).
11. Rathore, R. K., Kumar, N., Agnivesh Kumar, S., Sanjay Kumar, S., Sharma, A. K. & P. & and Mechanical properties of lightweight aluminium hybrid composite foams (AHCFs) for structural applications. *Adv. Mater. Process. Technol.* **8**, 4194–4208 (2022).
12. Amigó, V., Ortiz, J. L. & Salvador, M. D. Microstructure and mechanical behavior of 6061Al reinforced with silicon nitride particles, processed by powder metallurgy. *Scr. Mater.* **42**, 383–388 (2000).
13. Vijayakumar, R. et al. Optimization of wear process parameters of Al6061-Zircon composites using Taguchi method. *Adv. Mater. Sci. Eng.* **2023**, 1–10 (2023).
14. Cristofolini, I., Rao, A., Menapace, C. & Molinari, A. Influence of sintering temperature on the shrinkage and geometrical characteristics of steel parts produced by powder metallurgy. *J. Mater. Process. Technol.* **210**, 1716–1725 (2010).
15. Sinha, A. K., Rathore, R. K. & Bharti, S. A review on sliding wear of polymer composites. *AIP Conf. Proc.* **3111**, 060003 (2024).
16. Bolzoni, L., Ruiz-Navas, E. M. & Gordo, E. Influence of sintering parameters on the properties of powder metallurgy Ti–3Al–2.5V alloy. *Mater. Charact.* **84**, 48–57 (2013).

17. Masooth, H. S., Bharathiraja, P., Jayakumar, G., Palani, K. & V. & Microstructure and mechanical characterisation of ZrO2 reinforced Ti6Al4V metal matrix composites by powder metallurgy method. *Mater. Res. Express*. **9**, 020003 (2022).
18. Samal, C. P., Parihar, J. S. & Chaira, D. The effect of milling and sintering techniques on mechanical properties of Cu–graphite metal matrix composite prepared by powder metallurgy route. *J. Alloys Compd.* **569**, 95–101 (2013).
19. Anbuchezhiyan, G., Vignesh, M. & Shanmugam, V. Exploration of morphological and mechanical behaviour of Al2O3/Al-Mg-Cr-Zn alloy composites with Al6O13Si2 addition. *Mater. Lett.* **357**, 135696 (2024).
20. Vignesh, M., Anbuchezhiyan, G., Mamidi, V. K. & Vivek Anand, A. Enriching mechanical, wear, and corrosion behaviour of SiO2/TiO2 reinforced al 5754 alloy hybrid composites. *Mater. Lett.* **361**, 136106 (2024).
21. Satish, J. & Satish, K. G. Study of wear behaviour of magnesium hybrid metal matrix composites using Taguchi method. *AIP Conf. Proc.* **2274**, 030010 (2020).
22. Vijayakumar, R. et al. Optimization of Wear Process Parameters of Al6061-Zircon Composites Using Taguchi Method. *Advances in Materials Science and Engineering* 9507757 (2023). (2023).
23. Vignesh, M. et al. Influence of Cu and Co addition on metallurgical and wear characteristics of alcrfeni high entropy alloy. *Sci. Rep.* **14**, 27398 (2024).

Author contributions
G.A., V.M., E.N., and N.M.M. wrote the main manuscript text, and G.A., V.M., S.M., and P.B. prepared Figs. 1, 2, 3, 4, 5, 6, 7, 8, 9, 10 and 11; Tables 1, 2, 3, 4, 5, 6 and 7. All authors reviewed the manuscript.

Funding
The authors received no funding for this work.

Declarations

Competing interests
The authors declare no competing interests.

Additional information
Correspondence and requests for materials should be addressed to M.V. or N.M.M.

Reprints and permissions information is available at www.nature.com/reprints.

Publisher's note Springer Nature remains neutral with regard to jurisdictional claims in published maps and institutional affiliations.